Performance Analysis of the Slowed-Rotor Compound Helicopter Configuration

Matthew W. Floros
Raytheon ITSS
Moffett Field, California

Wayne Johnson
Army/NASA Rotorcraft Division
NASA Ames Research Center
Moffett Field, California

The calculated performance of a slowed-rotor compound aircraft, particularly at high flight speeds, is examined. Correlation of calculated and measured performance is presented for a NASA Langley high advance ratio test and the McDonnell XV-1 demonstrator to establish the capability to model rotors in such flight conditions. The predicted performance of a slowed-rotor vehicle model based on the CarterCopter Technology Demonstrator is examined in detail. An isolated rotor model and a model of a rotor and wing are considered. Three tip speeds and a range of collective pitch settings are investigated. A tip Mach number of 0.2 and zero collective pitch are found to be the optimum condition to minimize rotor drag. Performance is examined for both sea level and cruise altitude conditions.

Nomenclature

C_T	thrust coefficient
C_Q	torque coefficient
C_H	longitudinal inplane force coefficient
D	drag
L	lift
M_{TIP}	tip Mach number
V_T	tip speed
q	dynamic pressure
α_s	shaft angle
δ_3	rotor blade pitch-flap coupling angle
μ	advance ratio
ψ	rotor azimuth angle
σ	rotor solidity

Introduction

Recently there has been increased interest in expanding the envelope of vertical lift vehicles, particularly in terms of speed, altitude and range. Increased range allows attack, scout, and rescue vehicles to reach farther from their bases. Additional speed and altitude capability increases the survivability of military vehicles and cost efficiency of civilian aircraft. Long loiter times improve the effectiveness of scout aircraft, with particular applications of interest being unmanned aerial vehicles (UAVs) and homeland security surveillance aircraft.

Presented at the AHS 4th Decennial Specialists' Conference on Aeromechanics, San Francisco, California, January 21–23, 2004.

Much work has been focused on tilt rotor aircraft; both military and civilian tilt rotors are currently in development. But other configurations may provide comparable benefits to tilt rotors in terms of range and speed. Two such configurations are the compound helicopter and the autogyro. These configurations provide STOL or VTOL capability, but are capable of higher speeds than a conventional helicopter because the rotor does not provide the propulsive force or at high speed, the vehicle lift. The drawback is that redundant lift and/or propulsion add weight and drag which must be compensated for in some other way.

One of the first compound helicopters was the McDonnell XV-1 "Convertiplane," built and tested in the early 1950s. There were many novel design features in this remarkable aircraft (Refs. 1–4), which was tested in the NACA 40- by 80-Foot Wind Tunnel at the Ames Aeronautical Laboratory (Ref. 5) and flight tested near McDonnell's St. Louis, Missouri facilities (Ref. 6). The aircraft successfully flew in its three distinct operating modes, helicopter, autogyro, and airplane, and could transition smoothly between them.

One of the features of the XV-1 was that in airplane mode, the rotor would be slowed to a significantly lower speed to reduce its drag in forward flight. The combination of high forward speed and low rotor speed produced an advance ratio near unity, which is far above what is typical for conventional edgewise rotors.

Other prototype compound helicopters since the XV-1 include the Fairey Rotodyne and the Lockheed Cheyenne. Prototypes of both aircraft were built and flown, but never entered production. Recently, CarterCopters and Groen Brothers have developed autogyro demonstrators and have proposed auto-

gyros and compound helicopters for future heavy lift and unmanned roles.

The purpose of the current effort in the Aeroflightdynamics Directorate, US Army Aviation and Missile Research, Development and Engineering Center, is to examine the performance that can be expected from a slowed-rotor compound aircraft, particularly at high flight speeds. The performance was calculated using the comprehensive analysis CAMRAD II (Ref. 7). Correlation with historical high advance ratio test data is presented to establish the capability to model rotors in such flight conditions. Then the predicted performance of a slowed-rotor vehicle model based on the CarterCopter Technology Demonstrator (CCTD) is examined in detail.

High Advance Ratio Correlation

The data for the correlation were obtained from a high advance ratio test program at NASA Langley by Jenkins *et al.* (Refs. 8, 9) and from XV-1 wind tunnel data in References 5 and 10. These data sets are of interest not only because they provide high advance ratio data, but because they bear similarities to modern prototypes in development. In particular, the rotor used to collect the Jenkins data was a teetering rotor and both the Groen Brothers Hawk 4 and the CarterCopter Technology Demonstrator (CCTD) prototypes use teetering rotors. The XV-1 has a significantly different rotor system, but the overall vehicle is quite similar to the modern prototypes. Shared traits are the single main rotor, pusher propeller, and twin vertical tails with the horizontal stabilizer connecting them.

Correlation with NASA High Advance Ratio Test

The first set of data used for correlation was from the the high advance ratio test at NASA Langley reported in reference 9. A teetering rotor was tested at advance ratios ranging from 0.65 to 1.45. The variables measured were thrust, drag, power, and flapping angle at shaft angles of 0.5 degrees and 5.5 degrees (tilted backward relative to the oncoming wind). For the 0.5 deg shaft angle case, four advance ratios were tested; five were tested at 5.5 deg shaft angle.

The rotor properties are shown in Table 1. The rotor's simplicity makes it a good test article for correlation with analysis. The CAMRAD II model was set up to match the wind tunnel test conditions as closely as possible. Distributed properties for the rotor are not available, so it was modeled using rigid blades. The shaft angle was fixed and the rotor was trimmed to zero flapping. Like the wind tunnel test, rotor speed was also fixed, hence advance ratio was set by the free stream velocity. A rigid wake model was used to calculate the rotor inflow. No precone, undersling, or δ_3 were mentioned in reference 9, so these properties were assumed to be zero. The airfoil was the NACA 0012, so publicly available airfoil tables could be used in the analysis.

Table 1. Properties of the Jenkins high advance ratio test rotor (Ref. 9)

Number of Blades	2
Radius	7.25 ft
Chord	1.16 ft
Solidity	0.0968
Lock number	5.05
Twist	0 deg
Tip speed	110 ft/sec
Airfoil	NACA 0012
δ_3	0 deg

Plots of thrust with collective pitch at 0.5 and 5.5 deg shaft angle are shown in Figures 1 and 2. Since the data are relatively sparse, linear or quadratic lines were fit to the data to improve their readability relative to the predictions. An interesting trend is evident. As the advance ratio is increased above approximately 0.9–1.0, the trend of thrust with collective pitch reverses. At $\mu = 0.93$, there is almost no change in thrust with collective pitch, and as advance ratio increases, the thrust becomes more negative as collective pitch is increased. This control reversal is captured by CAMRAD II and the slopes of the calculated results match the curve fits very closely. There is, however, an offset in thrust between the predictions and the test data.

The source of the thrust offset in Figure 1 is unknown. It cannot be corrected by incrementing collective pitch because the thrust at $\mu = 0.93$ is nearly constant with collective pitch. Perturbations in shaft angle and (fixed) blade twist did not change the calculated thrust sufficiently to account for the offset. The errors are thought to be measurement errors rather than analysis errors given the intersection of the test data lines for the 0.5 deg plot. At zero collective and zero shaft angle, the untwisted rotor should produce zero thrust if trimmed to zero flapping. The shaft angle tested was small, 0.5 deg, so the lines should all cross near the intersection of zero collective and zero thrust. When CAMRAD II was run with zero shaft angle, the curves did cross at zero collective and zero thrust. The data cross at about 2.5 deg collective and about C_T of 0.001.

The correlation for the remaining test variables is similar for the 5.5 and 0.5 deg shaft angles, so only the 0.5 deg cases are shown. Torque is shown in Figure 3. As with thrust, there is an offset in the data, but the trends are again well captured by the analysis. The torque becomes increasingly negative with increasing collective pitch and advance ratio. The offset mirrors that from Figure 1. The data are offset to a higher torque and/or collective pitch setting. One difference is that the analysis results collapse near zero collective pitch, a local maximum, while the test data intersect at about 3 deg collective, as the torque is falling off.

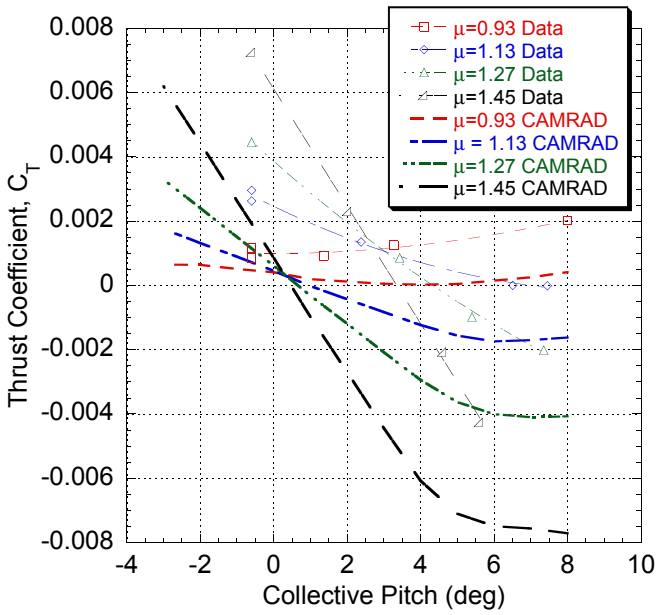

Fig. 1. Thrust correlation with high advance ratio data from reference 9, α_s = 0.5 deg.

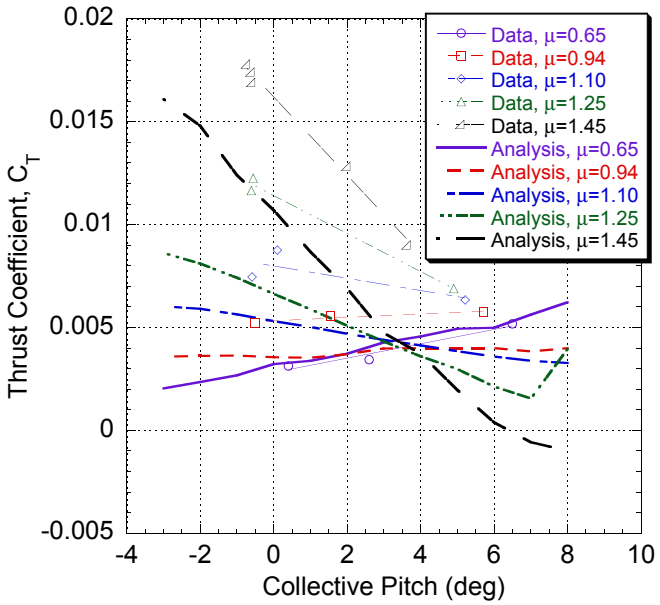

Fig. 2. Thrust correlation with high advance ratio data from reference 9, α_s = 5.5 deg.

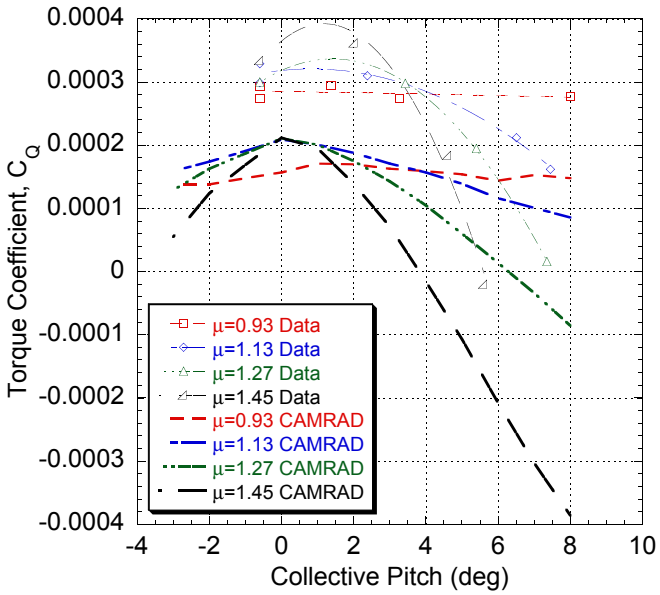

Fig. 3. Torque correlation with high advance ratio data, α_s = 0.5 deg.

Correlation of inplane force was less clear, but also encouraging. Figure 4 shows an approximately parabolic shape. The local minima predicted by CAMRAD II all occur near flat pitch while the inflection points in the data occur at several collective pitch settings. But the expected trend of inplane force increasing with advance ratio is evident in both the test data and the analysis. Moreover, the slopes of the CAMRAD II predictions at higher collective pitch settings approximate the slope of the data, particularly at the higher advance ratios. Also note that the drag coefficients are small, mostly clustered in the 0.001 range, so that small differences look larger as percent error.

Finally, longitudinal cyclic correlation is illustrated in Figure 5. Both the data and analysis predictions are approximately linear. Although the CAMRAD II predictions appear to be slightly higher, the lines are well within the scatter of the -0.5 deg collective pitch data points.

The conclusions from these results suggests that CAMRAD II can predict performance trends relatively well at high advance ratio using a rigid blade model. The rigid blade assumption is of course only accurate to the extent that the test hardware is stiff. The wake model is needed for performance calculations, but a rigid wake geometry is adequate at these high advance ratios.

Correlation with XV-1 Data

CAMRAD II was also used to correlate with the XV-1 Convertiplane full-scale rotor. This rotor is quite complex, but the complexities were not difficult to model in CAMRAD II.

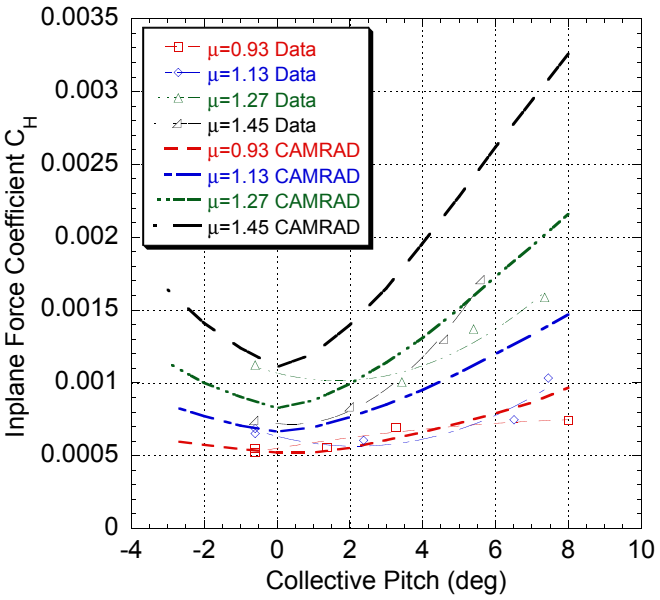

Fig. 4. Inplane force correlation with high advance ratio data, α_s = 0.5 deg.

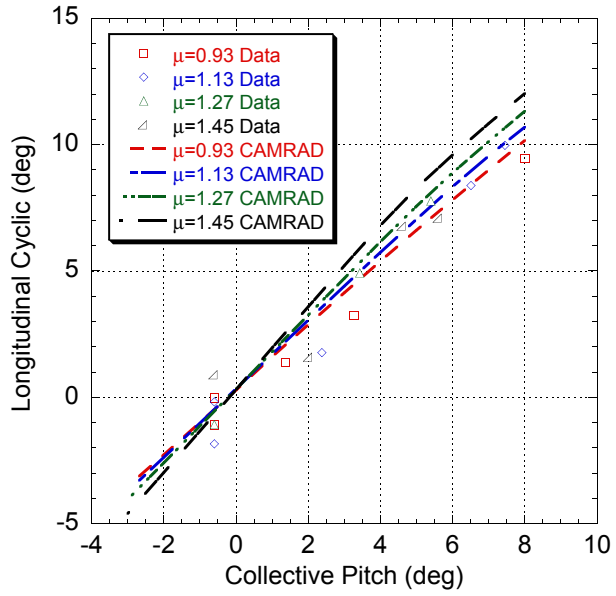

Fig. 5. Longitudinal cyclic pitch correlation with high advance ratio data, α_s = 0.5 deg.

Table 2. Properties of the McDonnell XV-1 convertiplane rotor

Number of Blades	3
Radius	15.5 ft
Chord	17.5 in
Solidity	0.09
Lock number	4.2
Twist	8 deg
Airfoil	NACA 63_2A(1.5)15
$\delta_{3,\text{gimbal}}$	15 deg
$\delta_{3,\text{coning}}$	65.6 deg

The rotor system had three blades and utilized both a gimbal and coning hinges on each blade to accommodate flapping (Ref. 1). The rotor properties are provided in Table 2 and Figure 6 shows a drawing from reference 11 that details the important hub components. The lag and centrifugal forces were reacted by metal retention straps with sufficient stiffness that the rotor was stiff inplane. Most of the pitch mechanism was contained inside the hub and pitch control was transmitted to the blades by means of a torque tube extending from the hub to the aerodynamic portion of each blade.

The rotor was designed to operate in three distinct flight regimes; helicopter, autogyro, and airplane mode. Helicopter mode was used for vertical takeoff and landing. The rotor was driven by tip jets and controlled by conventional collective and cyclic. Once the vehicle had sufficient forward speed, it would transition to autogyro mode, where the tip jets would be deactivated and the engine power would be transferred to the XV-1's pusher propeller. In autogyro mode, the rotor autorotates and slows from about 390 RPM to about 125 RPM as the vehicle increases speed. The pilot then pulls a lever to convert to airplane mode. In airplane mode, the hub lock ring (see Figure 6) engages the hub and locks out the gimbal. The hub pitch is then directly controlled by the stem labeled "cyclic pitch control" in Figure 6. In this mode, the rotor behaves like an articulated rotor as the blades flap about the coning hinges. The rotor is still autorotating, and a governor maintains 125 RPM by tilting the hub.

An interesting characteristic of the redundant articulation in the rotor hub is that there are two distinct values of pitch-flap coupling, δ_3. The gimbal has 15 deg of δ_3 while the coning hinges have 65.6 deg of δ_3. That corresponds to 2.2 deg of nose down pitch for every 1 deg of flapping at the coning hinge. The purpose of this large coupling is to keep the blades parallel to the hub at all times when the vehicle is in airplane mode.

Much of the wind tunnel test program (Ref. 5) was concentrated on full-scale development of the vehicle and hence little data were presented for the rotor only or for rotor and wing. Reference 10 describes an earlier test where a dummy

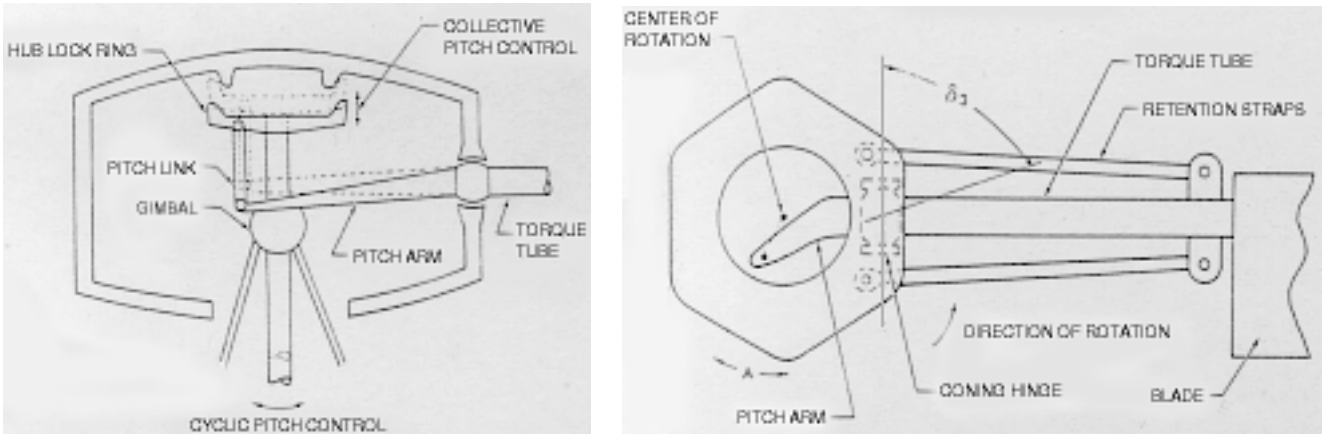

Fig. 6. Top and side view schematics of the XV-1 hub and blade assembly from reference 11.

fuselage and wing were tested with and without the rotor. By subtracting the data with only the wing and fuselage from the data with the rotor, wing, and fuselage, rotor-only data were obtained. The rotor-only data does not include interference effects from the dummy wing and fuselage.

Like the correlation with the Jenkins data, the analytical runs were configured to match the test conditions as closely as possible. For the results from reference 10, the rotor was trimmed to specific RPM settings for each data point. Therefore, in the CAMRAD II analysis, the rotor speed was specified and the trim procedure adjusted the shaft angle to achieve zero power (autorotation) on the rotor. Also, as in the Jenkins correlation, rigid blades were used in the analysis. The compressed air pipes for the tip burners forced the rotor blades to be thick and therefore stiff, so the rigid blade assumption is reasonable. Both the gimbal and coning hinge motion was allowed for autogyro flight comparisons.

One of the differences between the model and the test is the blade airfoil. Airfoil tables for the NACA 63_2A(1.5)15 were not available, so the more common NACA 23012 airfoil was used instead. In the test, the collective pitch was fixed to specified levels, 0 deg for airplane mode and 6 deg for autogyro mode. The collective could be shifted to account for differences between the two airfoils, but no adjustment to collective was required to match the test data. Although airfoil tables were not available for the NACA 63_2A(1.5)15, low speed data was available for the similar NACA $63_2$215 (Ref. 12). The low speed data showed that the NACA $63_2$215 has a zero lift angle of attack of approximately -1 deg, the same as the 23012.

Figure 7 shows CAMRAD II predictions of rotor lift in autogyro mode compared to the test data from reference 10. The data in this figure represent advance ratios between 0.2 and 0.4. The curves have approximately quadratic trend with rotor speed. The predictions in CAMRAD II lie nearly on top of the test data for the three rotor speeds.

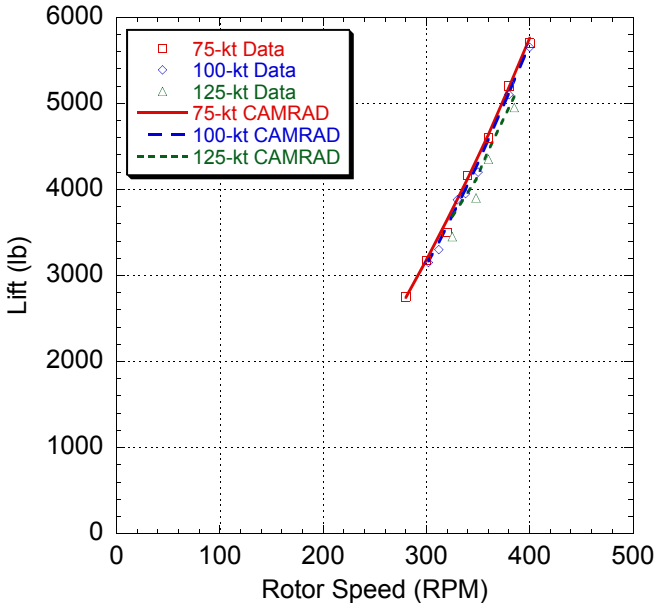

Fig. 7. Comparison of calculated XV-1 isolated rotor lift in autogyro mode and test data (reference 10).

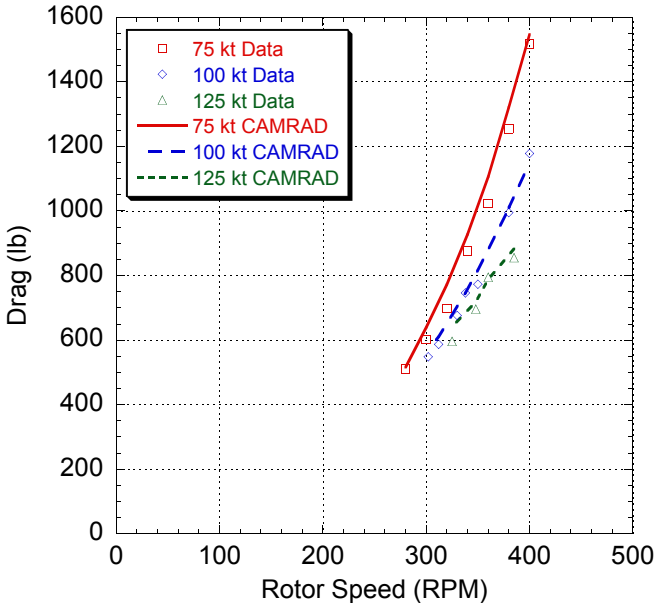

Fig. 8. Comparison of calculated XV-1 isolated rotor drag in autogyro mode and test data (reference 10).

Figure 8 shows the calculated and measured rotor drag in autogyro mode. Some adjustments were necessary to match the rotor drag. Initially, only the aerodynamic portion of the blade was modeled and the drag was under-predicted. The aerodynamic portion of the blade begins at 0.283R, and inboard of the attachment is a fairing over the torque tube and retention straps external to the fairing. One would expect that neglecting this amount of blockage would result in underprediction of rotor drag. No data were available for dimensions or aerodynamic properties of the fairing and straps, so a simple model was employed to produce equivalent drag. An aerodynamic fairing was added between the coning hinge and the blade clevis (0.062R to 0.283R) with the same chord as the aerodynamic portion of the blade. This fairing was assumed to have a drag coefficient of 0.08, independent of angle of attack and Mach number, and no lift or moment coefficients. This simple model significantly improved the correlation with test data. The resulting correlation is shown in Figure 8.

Slowed-Rotor Compound

A slowed-rotor vehicle model based on the CarterCopter Technology Demonstrator (Ref. 13) was developed to examine the performance of such a concept. Since little detailed information is publicly available about the prototype, the analytical model is relatively simple. It is intended only to capture the basic geometry of the aircraft, see Figure 9. The rigid blade analysis does not allow for elastic bending or torsion, so many details of the mass and stiffness distributions and aerodynamic center offsets would be obscured by the analysis even if they were available. Two models were used for analysis, a rotor only model and a model with a rotor and wing. The properties of both are shown in Table 3.

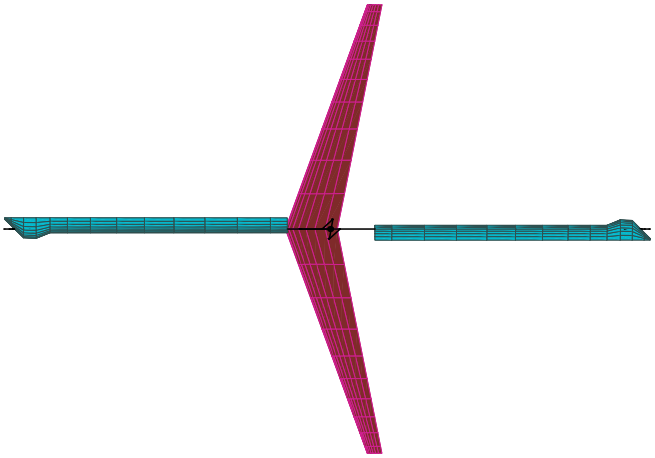

Fig. 9. Top view of CAMRAD II rotor and wing model, $\psi = 0$ deg, direction of flight to left.

The CarterCopter Technology Demonstrator is controlled only with collective pitch and spindle tilt. For the calculations, spindle tilt was modeled by tilting the rotor shaft. All calculations were made with zero cyclic pitch. An implicit trim condition for a teetering rotor is also that the hub moment must be zero. This condition is accommodated by flapping.

The prototype rotor has an extremely low Lock number caused by the presence of 65-lb uranium masses at the blade tips. These provide rotational inertia to store enough energy in the rotor for a jump take-off. The masses are located forward-slung in a triangular shape extending from the leading edge of each blade tip. Note that the chordwise location is of no consequence for the purposes of this study. The rigid blade model does not allow for elastic torsion and is hence insensitive to the chordwise mass distribution. For the purposes of this study, the sweep of the quarter chord due to the masses was ignored and only the chord width variation was modeled. This reduced the computation time and improved convergence behavior by eliminating direction changes in the bound vortices and aerodynamic panels which interact with trailed vortices in the wake model. Figure 10 shows the rotor with trailed vortices at an advance ratio of 1.0. With such a large reverse flow region, the trailed vortices overlap the blade on much of the retreating side, making wake convergence challenging.

For the actual aircraft, the blade airfoil changes from an NACA 65_4021 at the root to an NACA 65006 at the tip. Airfoil tables were not available for either of these sections, so the NACA 23012 was again used as a replacement.

The wing model is straightforward. The wing is swept, tapered, and untwisted, with an aspect ratio of 13.4. The aerodynamic model of the wing in CAMRAD II is identical to the aerodynamic model of the rotor blades. The only modeling

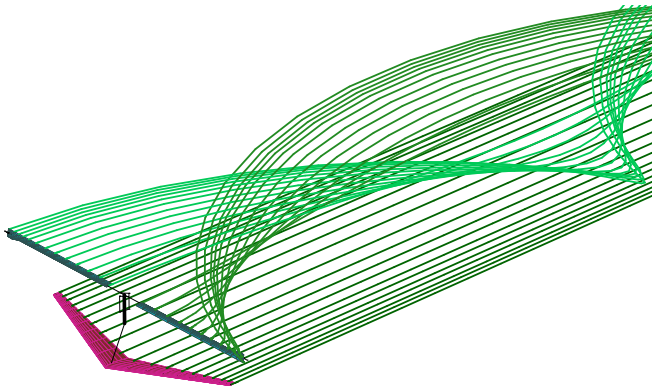

Fig. 10. Illustration of rotor and wing wake models for CCTD: rigid wake geometry at $\mu = 1.0$, $\psi = 90$ deg.

detail to note at present is again the use of the NACA 23012 airfoil as a replacement for the NACA $65_3$618. Details of trim with the rotor and wing are discussed in the results section following.

Isolated Rotor

To trim an autogyro, the procedure is different than that used for the high advance ratio correlation results. The rotor is unpowered, so the rotor speed is controlled by the free stream wind velocity and the angle of attack of the rotor. Two possibilities exist for trim. First, the orientation can be fixed and the rotor trimmed by adjusting RPM until a zero power condition is achieved. Alternatively, the RPM can be set and the the shaft tilt adjusted to achieve zero power. The latter was selected, because it is the more probable method of trim for a production aircraft. The pilot normally does not control the shaft tilt manually as manual shaft tilt would likely result in an unacceptable pilot workload. Instead, a governor or automatic control system maintains the desired RPM by tilting the shaft. This was how the XV-1 was operated in airplane mode.

The performance metrics of interest were drag and power, with power defined as the product of drag and velocity (this number would be divided by propeller efficiency to obtain the required propeller power). Individual components of rotor and wing power, such as induced and profile power were also examined.

Collective pitch and either the dimensional parameters rotor speed and velocity, or non-dimensional parameters hover tip Mach number and advance ratio, were varied to determine their effects on the drag and power. Hover tip Mach numbers of $M_{\mathrm{TIP}} = 0.2$, 0.3, and 0.4 correspond to rotor speeds of 100, 150, and 200 RPM or tip speeds of 230, 345, and 460 ft/sec at sea level. Although results are presented primarily in terms of hover tip Mach number, it is important to note that the three Mach numbers are all quite low and compressibility effects

Table 3. Properties of the CarterCopter rotor and wing

Rotor	
Number of Blades	2
Hub type	teetering
Radius	22 ft
Root chord	17 in
Tip chord	7 in
Solidity	0.032
Lock number	2.3
Twist	0 deg
Airfoils	variable NACA 65-series
δ_3	10 deg
Wing	
Span	32 ft
Root chord	45 in
Tip chord	12.5 in
Aspect ratio	13.4
Sweep angle	18 deg
Incidence angle	5.2 deg
Dihedral	6 deg
Wash out	none
Airfoil	NACA $65_3$618
Rel. Position	(8.9, 2.63) ft below, forward of rotor

were only seen at high speed even for the highest rotor speed. Figure 11 illustrates the relationship between the flight speed and rotor advance ratio for the three rotor speeds. At the highest rotor speed, the forward speed is above 250 kts before the advancing tip Mach number reaches 0.8. Sonic speed is not reached for any tip speed for the airspeeds in this study.

Power required at several collective pitch settings, forward speeds, and rotor speeds is shown in Figure 12 to show the relative effects. Here, the rotor power is plotted at the three tip Mach numbers and at three different forward speeds for each tip Mach number. This shows the effects of changing rotor speed, airspeed, and collective pitch setting on the same plot. In the analysis, the airspeed was specified in terms of advance ratio; the common dimensional airspeeds shown represent different advance ratios for each tip speed.

Figure 12 shows that the minimum power occurs at the minimum rotor speed for all aircraft speeds. However, the difference is not that large, even at 204 kts. If the higher tip speed is necessary to alleviate loads or stability problems at high advance ratio, only an additional 50 horsepower would be required between the lowest and highest rotor speeds.

Figure 12 also suggests that flat pitch is the most efficient collective pitch setting. For nearly all of the curves on the plot, there is a local minimum at 0 deg collective pitch. However, the exceptions are the slow rotor speeds, $M_{\mathrm{TIP}} = 0.2$. Here, the local minimum appears to be a higher collective pitch, particularly for the higher speeds.

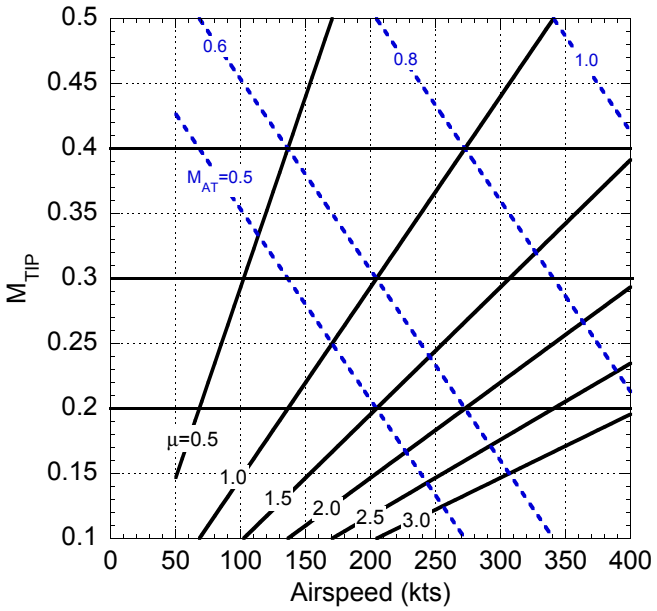

Fig. 11. Relationship between flight speed, hover tip Mach number, and advancing tip Mach number.

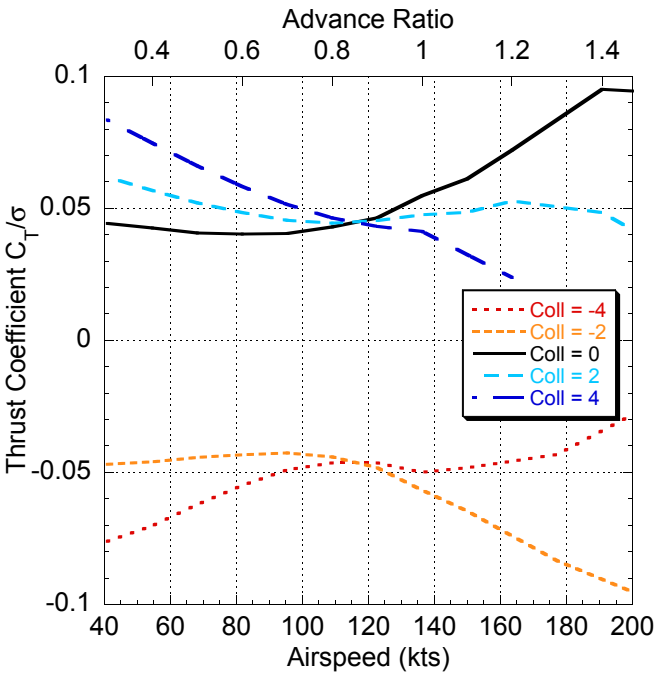

Fig. 13. Isolated rotor C_T/σ at -4 to 4 deg collective pitch, $M_{\mathbf{TIP}} = 0.2$.

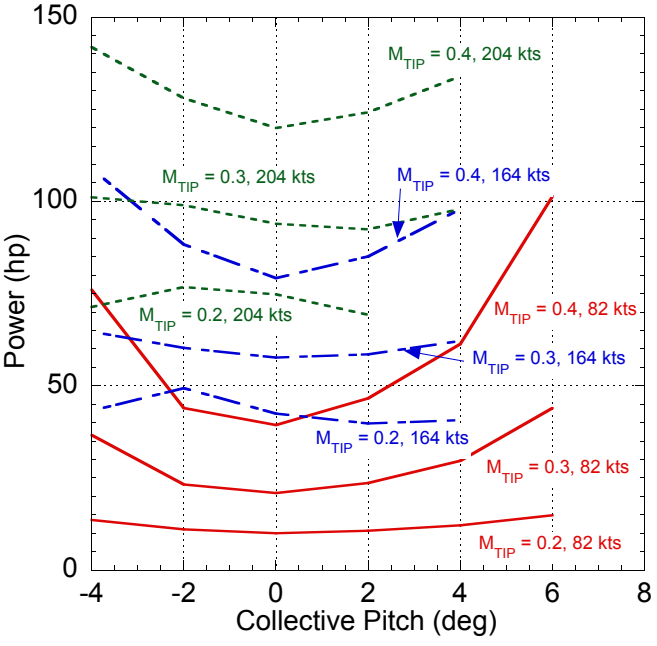

Fig. 12. Isolated rotor power with collective pitch at hover tip Mach numbers of 0.2, 0.3, and 0.4 and 82, 164, and 204 kts forward speed.

To illustrate the effect of collective pitch, the thrust behavior for a wider range of pitch settings is shown for $M_{\mathrm{TIP}} = 0.2$ in Figure 13. An interesting trend is evident, where the rotor thrust changes suddenly between 0 deg and -2 deg collective pitch. The reason for this is the autorotation condition of the rotor. In order for the rotor to autorotate, it must carry some lift, so as the rotor passes through zero lift, it must change condition suddenly to maintain autorotation. The NACA 23012 airfoil has a lift coefficient of zero at -1 deg angle of attack for low Mach numbers. Therefore, for an untwisted rotor, the condition change should occur near -1 deg collective. Indeed, the sudden change does occur between 0 and -2 deg collective in Figure 13.

More evidence is provided with the variation in the shaft angle required for trim, shown in Figure 14. Again, there is an abrupt change in the shaft angle trend between 0 and -2 deg collective pitch. Furthermore, the 0 and -2 deg lines are nearly symmetric about zero shaft angle, as are the +2 and -4 deg lines, at least above 80 kts. This further suggests that the lift reverses near -1 deg collective pitch. Beyond that, the combination of collective pitch, shaft angle, and airspeed provide the power to turn the rotor. Collective pitch, shaft angle, or both must provide the lift required to turn the rotor, with less required as airspeed increases. At flat pitch, the shaft angle starts at 5 deg and as airspeed increases, the shaft angle diminishes to nearly zero. At increased collective pitch settings, less shaft tilt is required to develop the required lift. At the negative collective pitch settings, the same trend is observed, but the shaft angle is tilted forward rather than back.

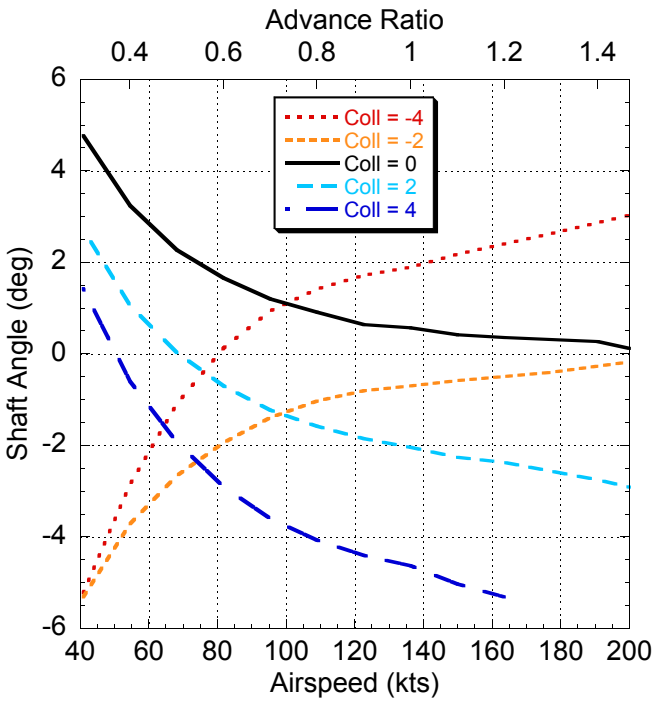

Fig. 14. Isolated rotor shaft angle at -4 to 4 deg collective pitch, $M_{TIP} = 0.2$.

Rotor and Wing

The purpose of modeling the rotor and wing together was to investigate how the two sources of vehicle lift interact with each other and share the vehicle weight, and how this, in turn, affects their individual performance. For the rotor and wing model, the trailed wake models of the wing and rotor are allowed to interact and influence each other.

Because performance was the focus of the present work rather than control, a simple trim condition was specified rather than a full six degree-of-freedom vehicle trim. The only requirements for trim were that the wing and rotor together lift the vehicle weight and that the rotor be autorotating (i.e. rotor power is zero). As in the isolated rotor analysis, for the purposes of CAMRAD II, the rotor RPM was specified and the shaft angle was a variable calculated by the analysis. The other variable was the incidence of the fuselage, which in turn specified the incidence of the wing. These two variables represent the fuselage angle of attack and spindle tilt of the CCTD. The vehicle gross weight was chosen to be 4200 lb, which is the maximum vertical takeoff weight of the CCTD. The rotor and wing are shown in Figure 9.

The distributions of rotor and wing lift are shown in Figure 15 for the three different rotor speeds. Looking at these three figures, the optimum collective pitch is 0 deg, as seen in the isolated rotor. At $M_{TIP} = 0.2$ and flat pitch (Figure 15a), the rotor lift required for trim increases some with speed; at $M_{TIP} = 0.3$ (Figure 15b), the increase is greater. For $M_{TIP} = 0.4$, the rotor lift is greater than the wing lift above 310 kts.

At negative pitch, for all three tip Mach numbers, the rotor in autorotation trims at negative thrust and the thrust becomes increasingly negative as advance ratio increases. This means that the the wing must carry additional lift to compensate for the rotor. Clearly that is not a desirable trim condition for the vehicle. The M_{TIP}=0.2 case has an interesting event near $\mu = 2.0$, where the trim rotor lift suddenly changes to approximately -1700 lbs as it requires more (negative) lift to simultaneously satisfy the zero power and zero hub moment requirements of an autorotating teetering rotor.

The positive 2 deg collective case changes behavior over the three tip Mach numbers. In Figure 15a, as forward speed increases, the rotor lift changes sign so that at high speed the rotor and wing are opposing each other. In Figure 15b, the curves diverge slightly, but are still sharing positive lift up to the maximum speed shown. At the highest tip Mach number, Figure 15c, the behavior is similar to that at flat pitch; the curves cross and separate rapidly.

These trends provide guidance for selecting rotor speed and collective. For positive collective pitch settings, the wing carries positive lift to a higher airspeed as rotor speed decreases. At a given rotor speed, more collective pitch causes the wing to carry more lift at higher speed, until point where the lift changes rapidly and the rotor and wing oppose each other. The fact that the rotor and wing work together beneficially over such a small collective range implies that controlling the rotor speed may be difficult even with an automatic control system and should be examined in detail. Such an investigation is beyond the scope of this paper.

Total and induced rotor power are shown in Figure 16. For each of the plots, it is clear that profile power dominates the rotor power. Induced power is comparatively small except for the highest rotor speed (Figure 16c), where the lift is large. At that rotor speed, compressibility has a significant effect on the blade drag, which results in more rotor lift and in turn higher induced power. At negative collective pitch settings, the induced power is particularly high. For the lowest rotor speed, Figure 16a, the power is nearly unchanged with collective, and collective pitch effects for the moderate rotor speed are relatively minor as well. A more detailed discussion of rotor power is provided later.

The rotor angle of attack is shown in Figure 17. This is the angle of the hub relative to the oncoming wind, similar to the isolated rotor shaft angle in Figure 14, not the tip path plane angle. Since there is no cyclic pitch, the hub plane is also the plane of no feathering. The trends should and do look similar to those for the isolated rotor in Figure 14. The shaft angle decreases for positive collective and increases for negative collective as the speed is increased.

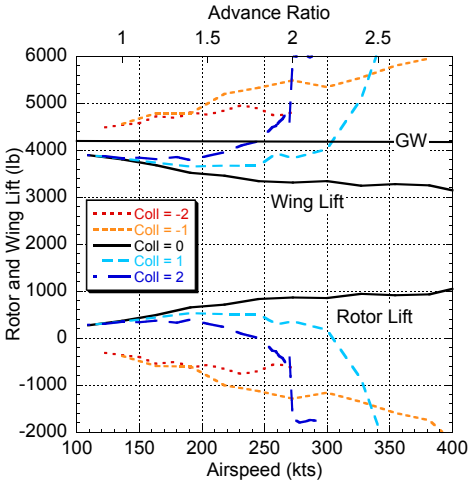

(a) $M_{\mathrm{TIP}} = 0.2$

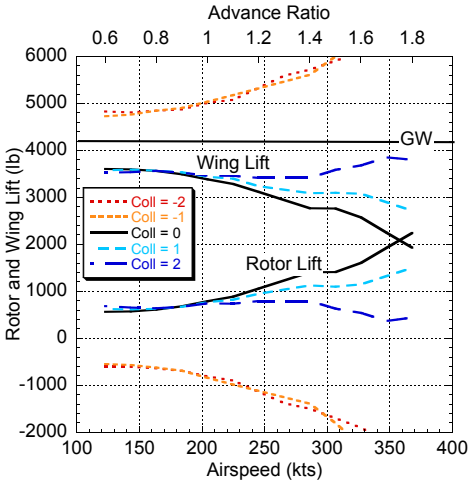

(b) $M_{\mathrm{TIP}} = 0.3$

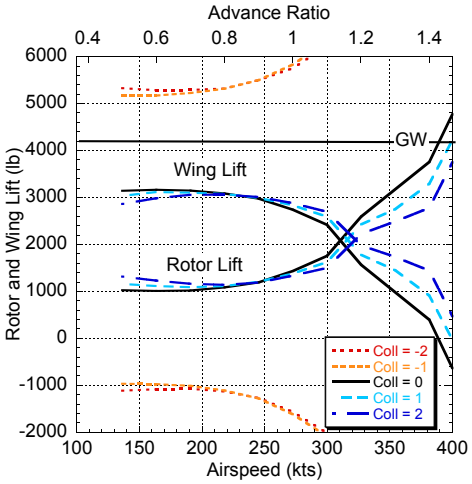

(c) $M_{\mathrm{TIP}} = 0.4$

Fig. 15. Lift of rotor and wing vs. airspeed from -2 to 2 deg collective, $0.2 \leq M_{\mathrm{TIP}} \leq 0.4$.

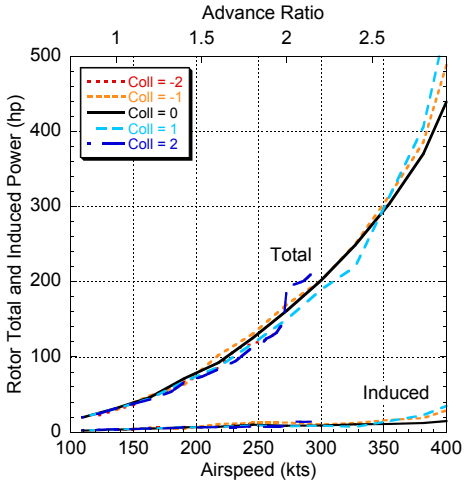

(a) $M_{\mathrm{TIP}} = 0.2$

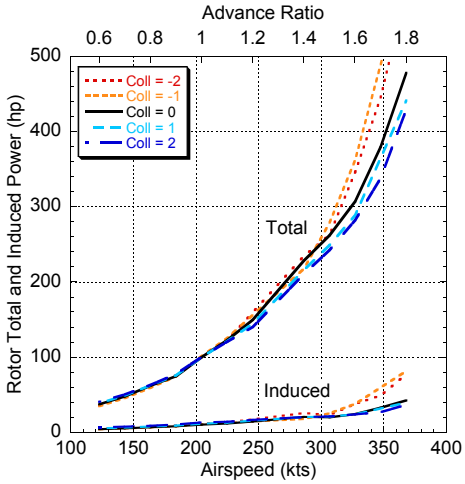

(b) $M_{\mathrm{TIP}} = 0.3$

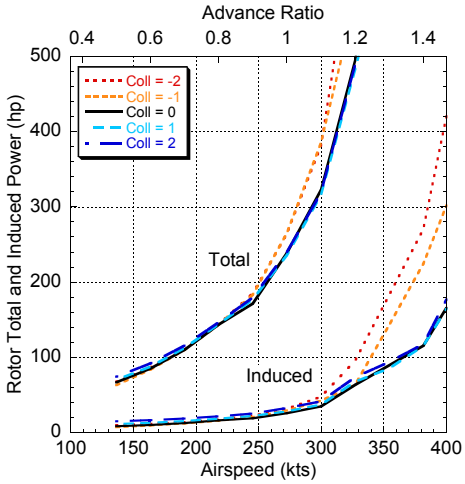

(c) $M_{\mathrm{TIP}} = 0.4$

Fig. 16. Total and induced rotor power vs. airspeed from -2 to 2 deg collective, $0.2 \leq M_{\mathrm{TIP}} \leq 0.4$.

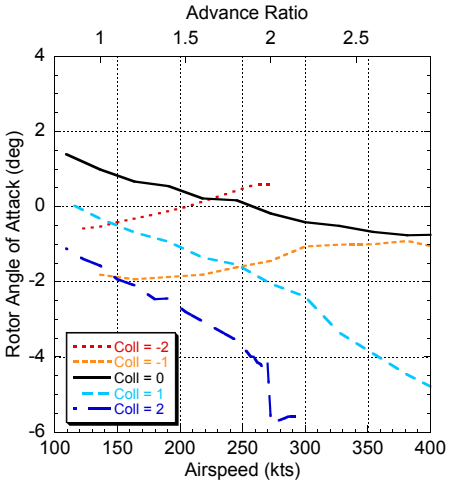

(a) $M_{\mathrm{TIP}} = 0.2$

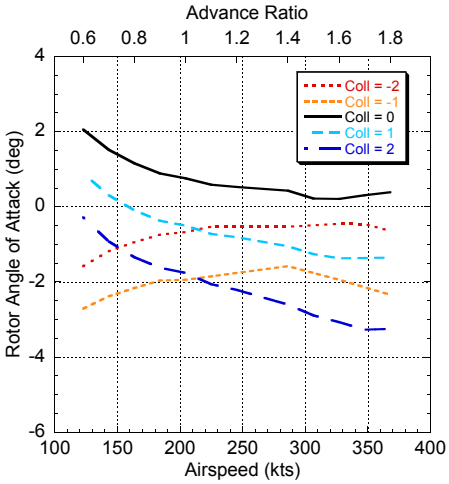

(b) $M_{\mathrm{TIP}} = 0.3$

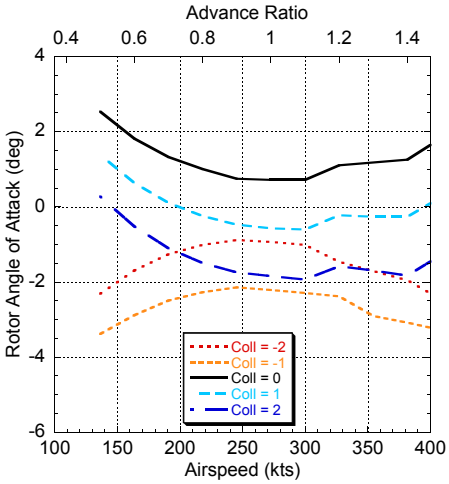

(c) $M_{\mathrm{TIP}} = 0.4$

Fig. 17. Rotor shaft angle vs. airspeed from -2 to 2 deg collective, $0.2 \leq M_{\mathrm{TIP}} \leq 0.4$.

The wing angle of attack in Figure 18 looks like one would expect from a fixed-wing aircraft without a rotor. At low speeds, the wing must maintain a large angle of attack to carry its share of lift, but as speed increases, the wing angle of attack asymptotically approaches zero. A closer examination shows the consistencies with Figure 15. First, the negative collective pitch settings require the wing to carry much higher lift in Figure 15. This results in a 2–5 deg increase in angle of attack in Figure 18. Also, the behavior of the 1 and 2 deg collectives in Figure 15a produce increased angles of attack in Figure 18a. Finally, the crossing of wing and rotor lift for 0 and positive collective pitch settings in Figure 15c result in negative angles of attack at high speed in Figure 18c. Note that the wing incidence relative to the fuselage is included in Figure 15, which shows the angle between the wing and the oncoming wind. Angles of attack below -1 deg result in negative lift.

Spindle tilt results are shown in Figure 19. The spindle tilt is shown as an indication of control requirements. Based on Figure 19a, the wing incidence appears to be consistent with the lowest rotor speed and flat pitch. For that condition, the spindle travel is symmetric about the undeflected position. For increasing tip speeds the shaft should be tilted with respect to the fuselage by about 2 and 5 deg, respectively for M_{TIP} of 0.3 and 0.4. The travel is at most 15 deg, even for the negative collective pitch settings. The separation between the 0 and -1 deg collective lines accentuates the control issue mentioned earlier. If the optimum collective pitch is zero, there is very little tolerance for changes in thrust from elastic twist or inflow changes. A spindle actuator maintaining rotor speed would have to move the spindle very quickly between 5 and 10 deg depending on rotor speed and airspeed.

The longitudinal flapping angles are shown in Figure 20. These, in combination with the rotor angle of attack in Figure 17, provide information about the tip path plane angle of the rotor. Looking at each plot individually, the flapping is approximately constant with airspeed at the low rotor speed and as rotor speed increases, airspeed dependence increases. At M_{TIP} of 0.2, the flapping changes only as the lift diverges at positive 1 and 2 deg collective pitch and the other collective settings have nearly constant flapping. In contrast, at M_{TIP} of 0.4, there is approximately a 5 deg difference in flapping over the airspeed range. The most dramatic difference is seen between the positive and negative collective pitch conditions in this figure. It reiterates the severity of the condition change between positive and negative collective pitch settings. Not only must the spindle tilt 5–10 deg, but the rotor flapping must change from about 8 to as much as 15 deg.

The preceding discussion has demonstrated that lower rotor speed improves performance and that zero deg collective pitch is the best condition at any speed. Now these trends are examined in more detail to reveal the physics behind them and clarify the role of the wing in the performance of the rotor and the total vehicle.

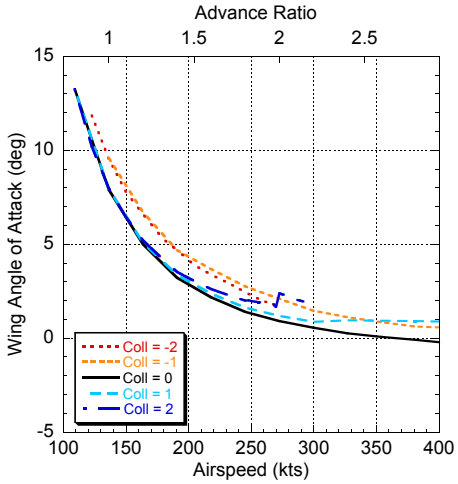

(a) $M_{\text{TIP}} = 0.2$

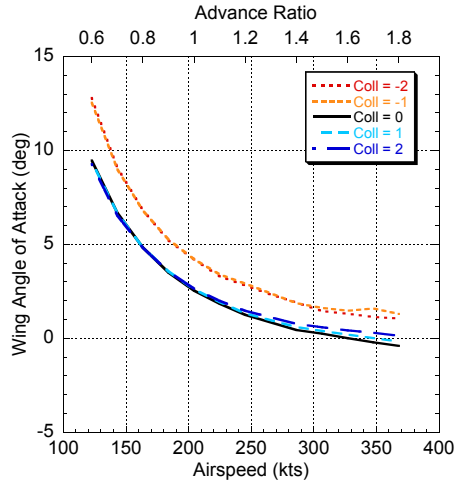

(b) $M_{\text{TIP}} = 0.3$

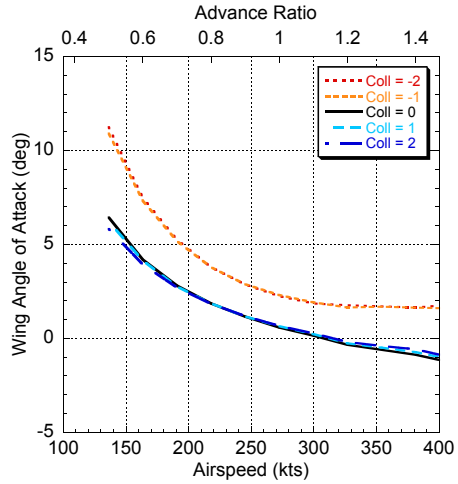

(c) $M_{\text{TIP}} = 0.4$

Fig. 18. Wing angle of attack vs. airspeed from -2 to 2 deg collective, $0.2 \leq M_{\text{TIP}} \leq 0.4$.

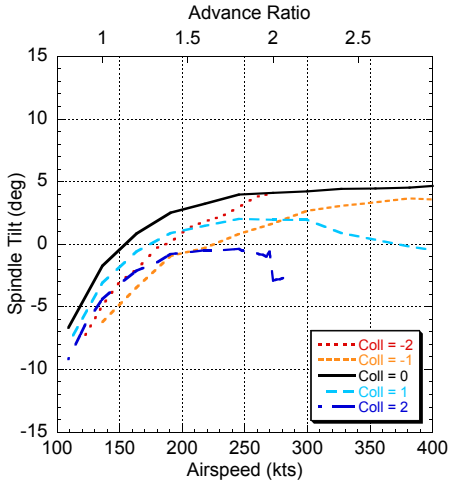

(a) $M_{\text{TIP}} = 0.2$

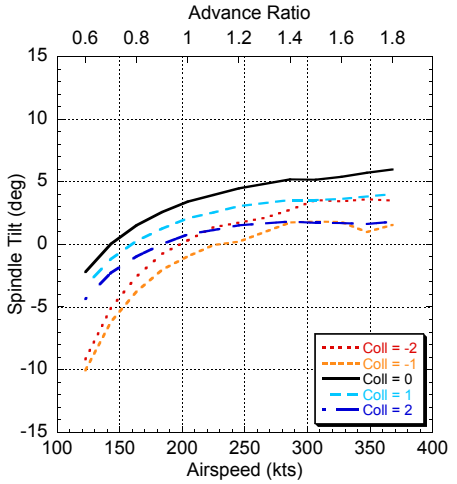

(b) $M_{\text{TIP}} = 0.3$

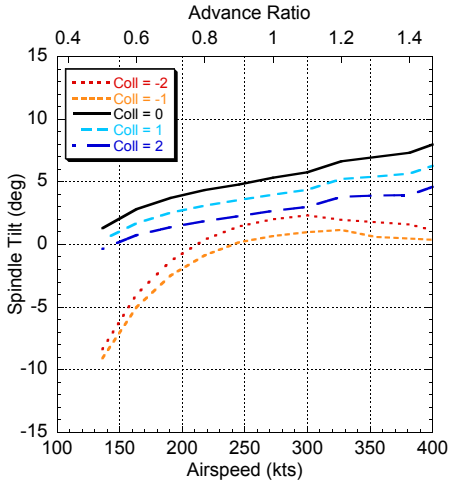

(c) $M_{\text{TIP}} = 0.4$

Fig. 19. Spindle tilt vs. airspeed from -2 to 2 deg collective, $0.2 \leq M_{\text{TIP}} \leq 0.4$.

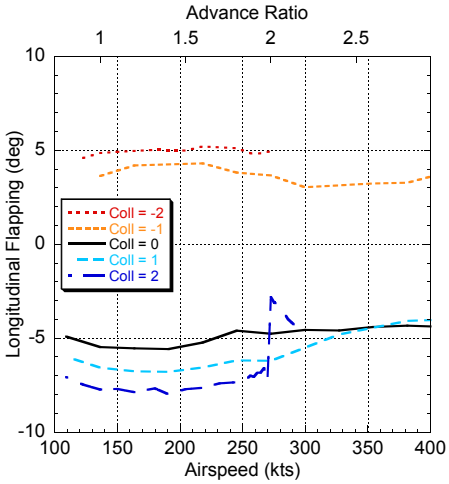

(a) $M_{\mathrm{TIP}} = 0.2$

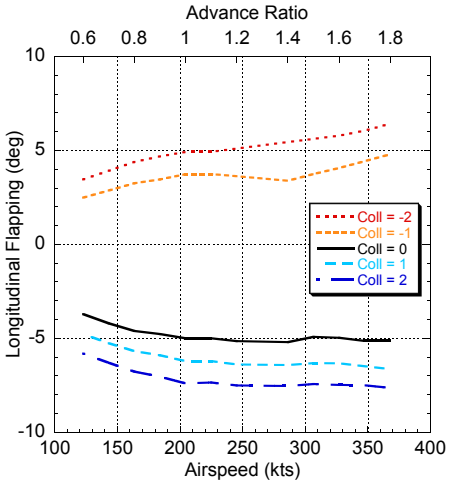

(b) $M_{\mathrm{TIP}} = 0.3$

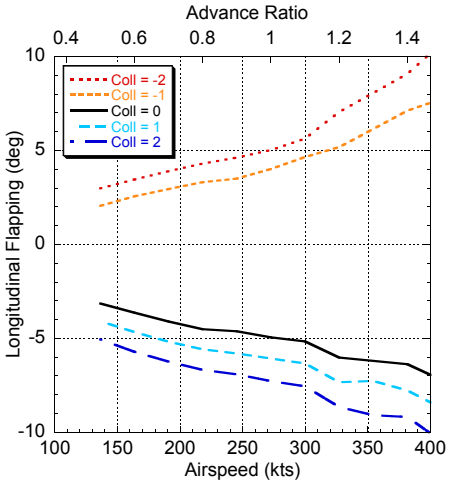

(c) $M_{\mathrm{TIP}} = 0.4$

Fig. 20. Longitudinal flapping vs. airspeed from -2 to 2 deg collective, $0.2 \leq M_{\mathrm{TIP}} \leq 0.4$.

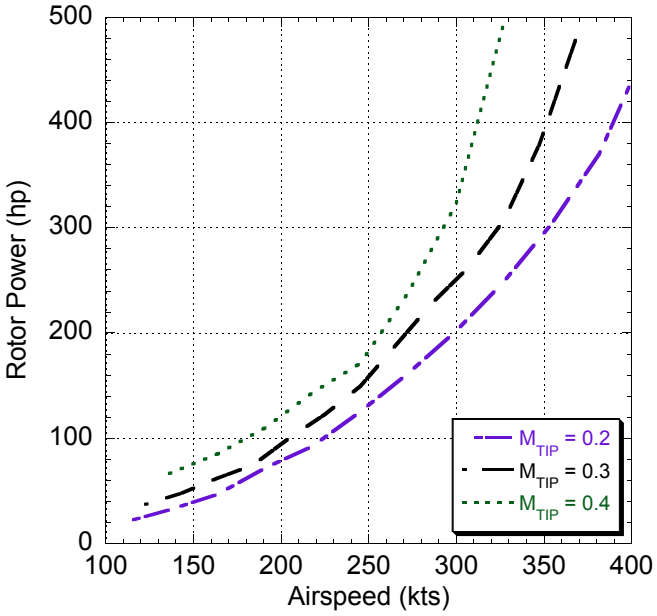

Fig. 21. Rotor power at tip Mach numbers of 0.2–0.4, 0 deg collective pitch.

Figure 21 shows rotor power at flat pitch for the three tip speeds. This more clearly shows the effect of rotor speed than Figure 16. The power increases with increasing rotor speed, and the difference widens as the vehicle speed increases. As stated earlier, three factors are at work increasing power required with M_{TIP}; the profile power is increasing, the induced power is increasing as more lift is required to overcome the profile power, and the blade drag increases as a result of compressibility.

The effects of compressibility are illustrated in Figures 22 and 23. Here, the rotor power and lift are compared with dimensional tip speeds of 230 ft/sec and 460 ft/sec, and tip Mach numbers of 0.2 and 0.4. To separate the effects of advance ratio and Mach number, a third line is added where the speed of sound was artificially increased by a factor of two such that the tip Mach number of the 460 ft/sec rotor speed matched that of the 230 ft/sec rotor speed.

In Figure 22, the difference between the two $M_{\mathrm{TIP}} = 0.2$ lines indicates that the profile power increase is resulting from rotor speed. The difference between the two 450 ft/sec lines illustrates the effect of compressibility, specifically the drag coefficient of the blade increasing with Mach number. Note that the profile drag increase caused by Mach number produces a direct profile power increase and an indirect increase in induced power just as the rotor speed increase does.

Figure 23 shows the influence of compressibility on the rotor lift. The rotor lift increases with speed in order to maintain autogyro trim, because the rotor power is increasing. At $M_{\mathrm{TIP}} = 0.4$, a large part of the power increase is attributed to the compressibility effects on profile power.

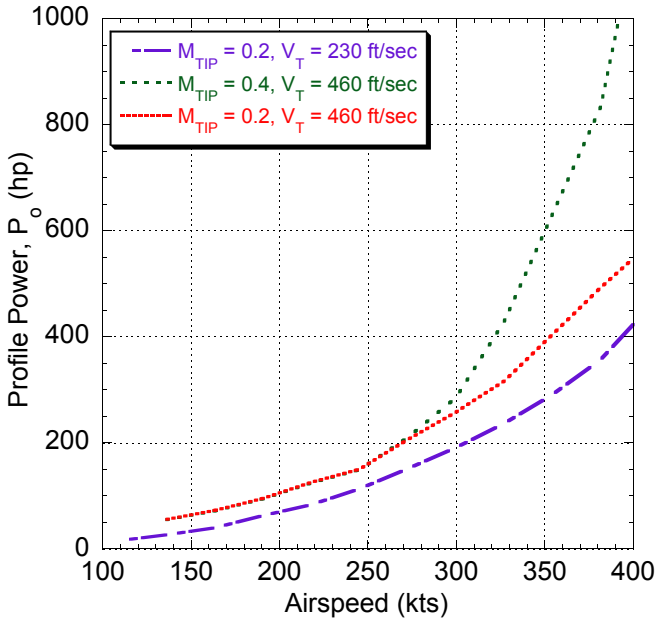

Fig. 22. Effect of compressibility on rotor profile power, 0 deg collective, M_{TIP}= 0.2, 0.4, and V_T = 230 and 460 ft/sec.

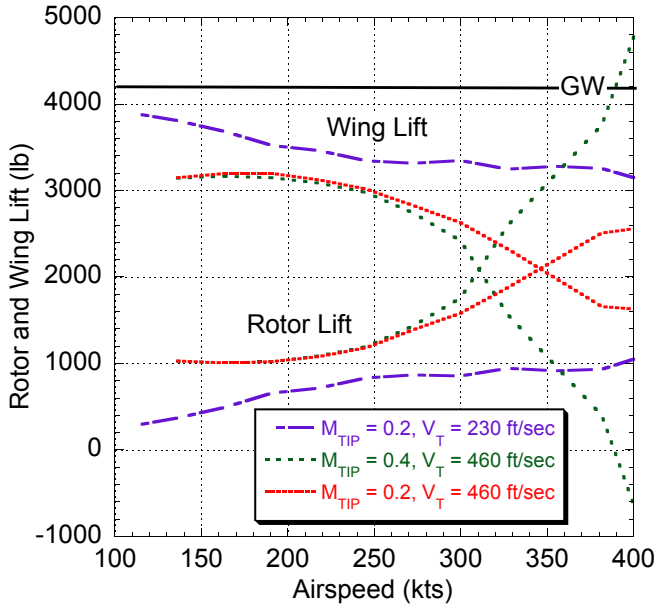

Fig. 23. Effect of compressibility on wing and rotor lift, 0 deg collective, M_{TIP}= 0.2, 0.4, and V_T = 230 and 460 ft/sec.

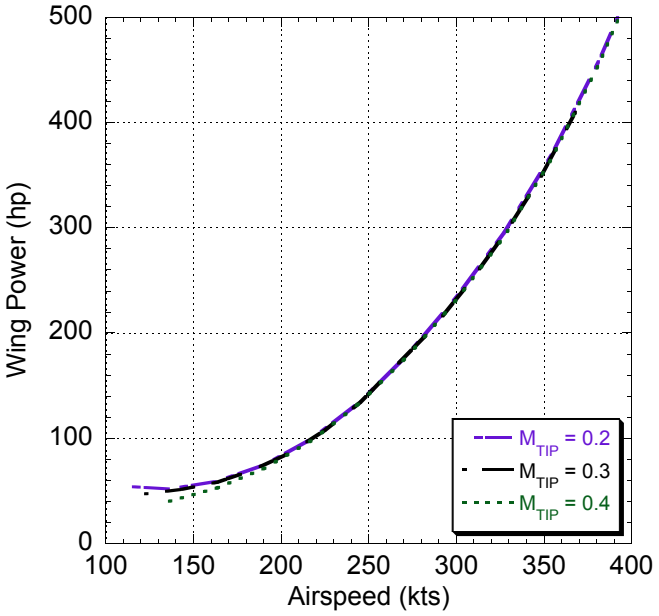

Fig. 24. Wing power at tip Mach numbers of 0.2–0.4, 0 deg collective pitch.

The wing is unaffected by the rotor speed, so its power required changes only to the extent that the sharing of lift between the wing and rotor changes. In Figure 24, the wing power is almost exactly the same for the three rotor speeds. The wing angle of attack, shown in Figure 25, changes very little with rotor speed, except at very low airspeed. At moderate and high airspeed, even small changes in the wing angle of attack produce substantial changes in the wing lift. At the lowest speeds, below 150 kts, the wing is operating very near stall. Increased rotor speed requires the rotor to generate more lift to maintain autorotation, unloading the wing. The increased discrepancy in wing angle of attack with rotor speed below 150 kts results from this difference in rotor lift.

The vehicle power is shown in Figure 26. Because the wing power is nearly insensitive to the rotor speed, the vehicle power looks similar to the rotor power in Figure 21. The scale is different, but the gradually widening increase in power required with increasing rotor speed is still clear.

Also notable in Figures 21, 24, and 26 is that the power required by the rotor is the same level as that of the efficient, high aspect ratio wing, at least at the low rotor speeds. At $M_{\mathrm{TIP}} = 0.4$, the power curves are very steep, so it is more difficult to compare them to the wing. For the lowest rotor speed, the rotor requires about 450 hp at the highest speed and the wing requires just over 500 hp. Noting that the wing is carrying over 75% of the lift (Figure 15), this is substantial power increase over a fixed wing, and quantifies the trade-off between vertical takeoff capability and cruise efficiency.

The interference power is also shown in Figure 26. The interference power is a measure of how the interaction of the

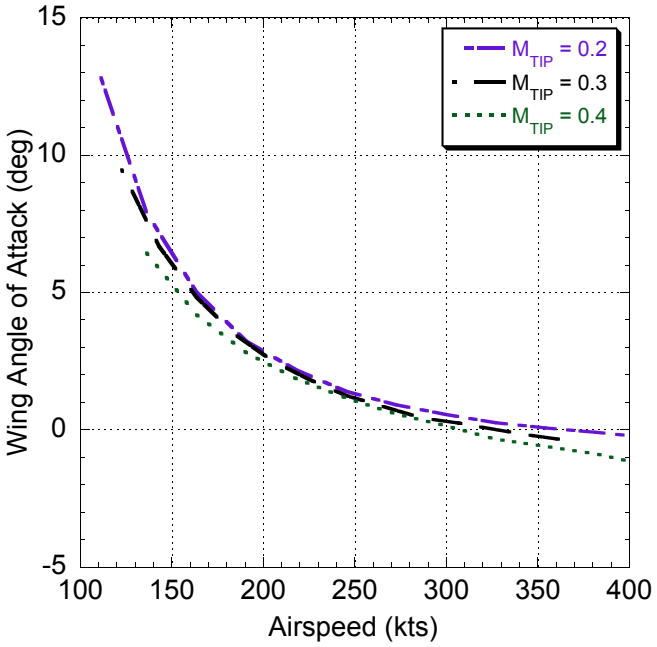

Fig. 25. Wing angle of attack at tip Mach numbers of 0.2–0.4, 0 deg collective pitch.

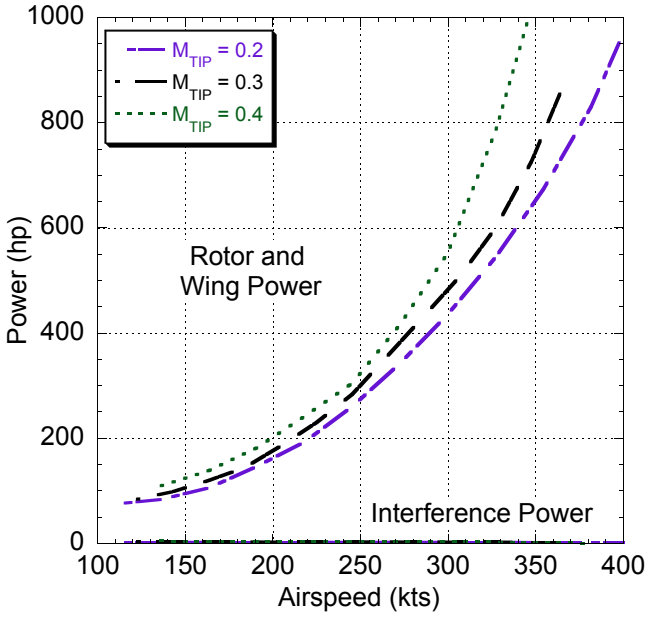

Fig. 26. Total and interference power of rotor and wing at tip Mach numbers of 0.2–0.4, 0 deg collective pitch.

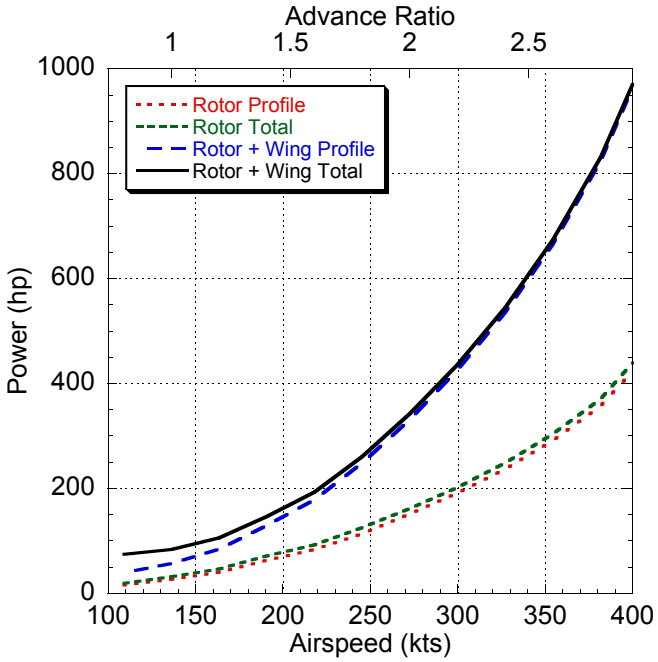

Fig. 27. Relative magnitudes of profile and induced power of wing and rotor, 0 deg collective, M_{TIP}= 0.2.

rotor and wing wakes adversely affect the lift on each lift device. The extremely low interference power indicates that the wing and rotor are separated by sufficient distance that they are essentially isolated from each other. The advance ratio scales on Figures 16-20 illustrate that the lowest advance ratio for the rotor is 0.5, which is very high for a helicopter and the wake is swept back far behind the vehicle before it interacts with the wing wake.

The relative importance of profile and induced power for both the wing and rotor is difficult to ascertain from the preceding discussion. A buildup of power for the lowest tip speed is shown in Figure 27. The grouping of the lines indicates that induced power is a minor contributor for both the rotor and the wing. The lines “profile” and “total,” showing profile with induced and interference power, are nearly indistinguishable. The sharing of power between the rotor and wing is also more clear as the distance from the x-axis to the rotor only lines is about the same as that to the rotor + wing lines.

The rotor incidence information is shown in Figures 28 and 29. The tip path plane angle is determined by the rotor angle of attack and longitudinal flapping. Spindle tilt is a control parameter and does not provide additional performance information, but is included along with lateral flapping for completeness.

The angle of attack and flapping are relatively constant with rotor speed. There is some variation with tip Mach number, but it only amounts to a degree or two. The comparatively large change in spindle tilt is accounting for the change in the

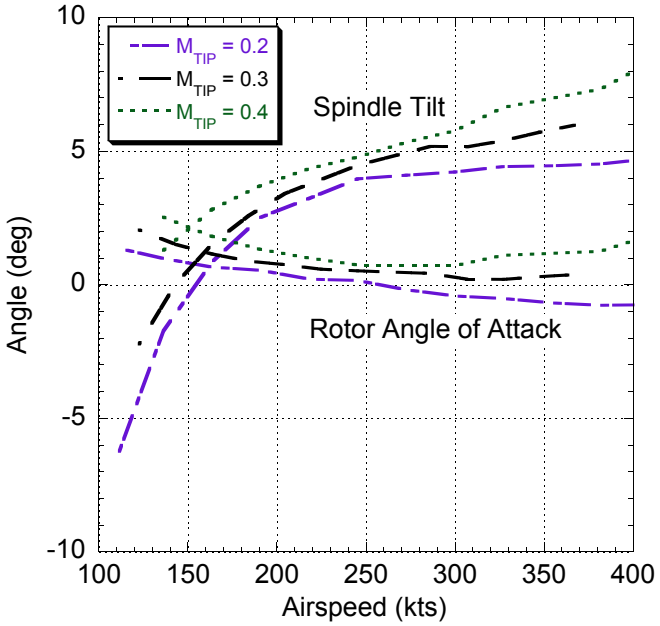

Fig. 28. Rotor hub angle and spindle angle at tip Mach numbers of 0.2–0.4, 0 deg collective pitch.

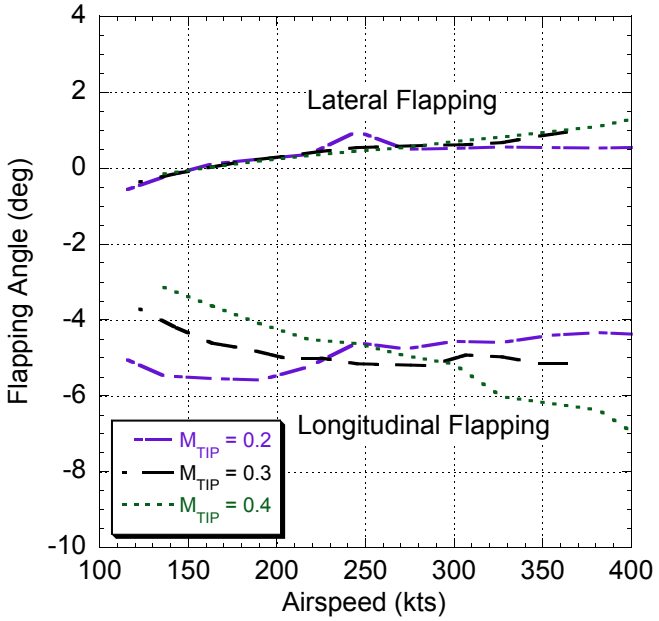

Fig. 29. Rotor flapping angles at tip Mach numbers of 0.2–0.4, 0 deg collective pitch.

wing angle of attack as speed increases. It negates the vehicle attitude change to keep the rotor at a nearly constant angle relative to the oncoming wind (Figure 28).

Having examined the rotor and wing performance in detail, consideration of the wing and rotor system performance is appropriate. Vehicle efficiency is commonly expressed in terms of lift-to-drag ratio, L/D. The L/D of the rotor and wing together and the wing alone are shown in Figure 30. At low rotor speed and low airspeed, the lifting system L/D is as high as 20. The efficient, high aspect ratio wing exceeds 30, indicating the relative amount of drag produced by the rotor at low speed. As the speed increases, though, and profile drag increases, the L/D of the wing/rotor combination decreases. This provides some insight into the degree to which the rotor drag can be reduced at high speed. It is important to note however, that these calculations do not include any sort of fuselage, so the drag and power calculations are not indicative of what the vehicle performance might be.

Another performance metric is D/q, the drag divided by the dynamic pressure. This indicates an equivalent flat plate area and is most useful for the fuselage, but is also useful to compare drag of lifting surfaces. The D/q of the wing and rotor system is shown in Figure 31. It shows that the power at high speed results primarily from the large dynamic pressure. When the dynamic pressure is removed, the equivalent flat plate drag is only about 1.5 square feet for the lowest rotor speed.

Also, interestingly, the effect of compressibility is evident in the $M_{\mathrm{TIP}} = 0.4$ case. D/q at the lower rotor speeds asymp-

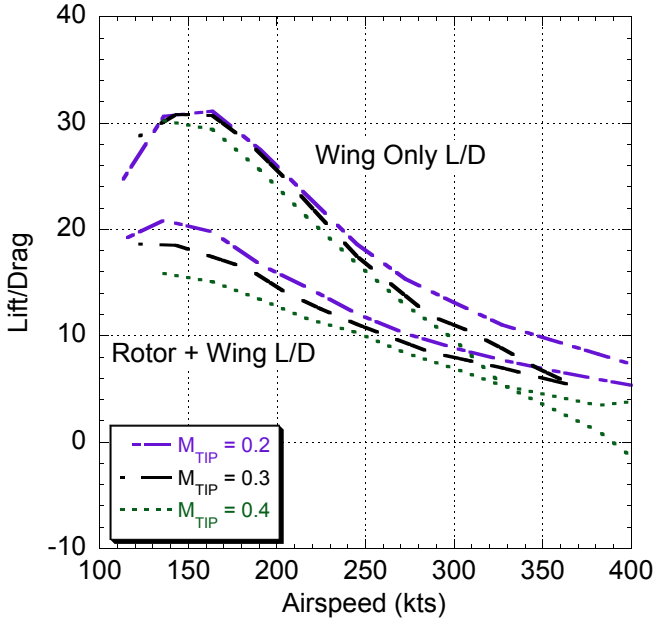

Fig. 30. Combined rotor and wing L/D at tip Mach numbers of 0.2–0.4, 0 deg collective pitch.

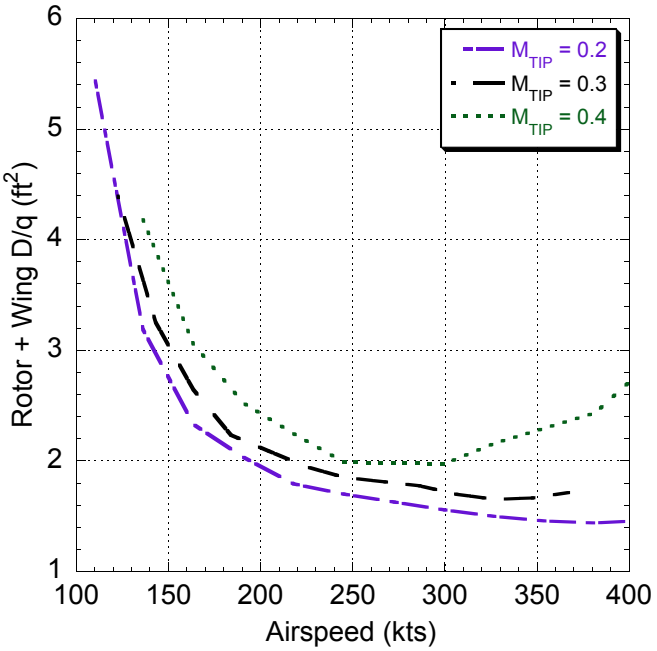

Fig. 31. D/q of rotor and wing at tip Mach numbers of 0.2–0.4, 0 deg collective pitch.

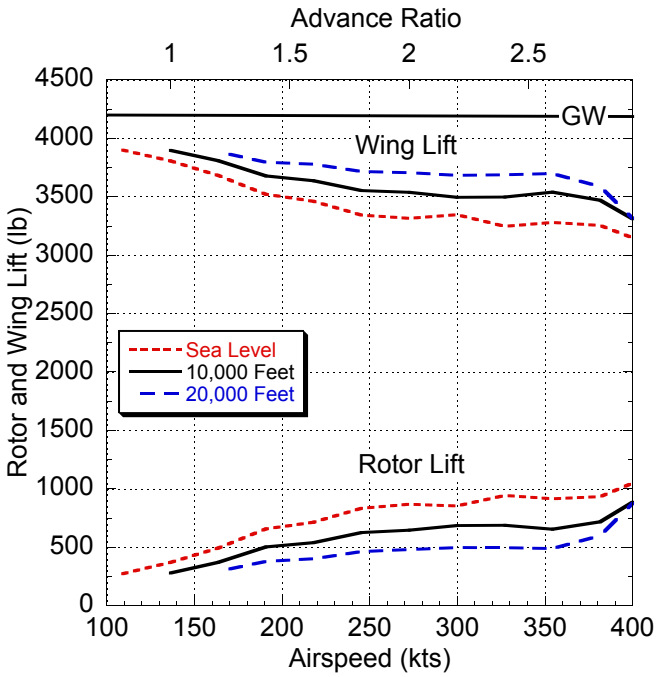

Fig. 32. Lift of rotor and wing from sea level to 20,000 feet, 0 deg collective, V_T = 230 ft/sec.

totically approach horizontal as speed increases, but at the highest rotor speed increases above 300 kts. Figure 31 indicates that compressibility results in a drag increase of approximately 70%.

One of the drivers for going from a conventional helicopter to a compound helicopter or another vertical lift configuration is that of high altitude performance. A pure helicopter normally stalls at high altitude, but the lifting wing considerably increases the service ceiling. Up to this point, calculations were made for sea level conditions. These will now be compared to high altitude to show the effect on the compound helicopter. The performance was calculated for standard conditions at sea level, 10,000 feet, and 20,000 feet altitude. For a tip speed of 230 ft/sec, the corresponding tip Mach numbers for these altitudes are 0.206, 0.214, and 0.222.

Sharing of lift, shown in Figure 32, is moderately affected. For most of the speed range, an additional 500 lbs per 10,000 feet is offloaded from the rotor to the wing. Figure 15(b) and (c) show the lift crossing and then diverging. The extreme right of Figure 32 indicates that this crossing is slightly different for each altitude, but is above the airspeeds of interest.

The combination of lift redistribution and the reduced air density at high altitude has a strong influence on the rotor and wing power. A breakdown of power, shown in Figure 33, indicates the power is reduced by more than 1/3 from sea level to 20,000 feet. The difference of 1/3 at the highest speed is nearly the same between the two, suggesting that the primary driver is the reduced air density. The reduction in power of the wing and rotor combined is slightly more than for the wing alone, however. The difference is because lift was transferred from the rotor to the wing. At low speed, the high induced power obscures any effects of altitude on profile power.

The L/D ratios for the wing and the rotor-wing combination are shown in Figure 34. The L/D illustrates the same points as power. For the wing alone, the peak L/D is about 31 and is independent of altitude. Sailplane pilots know well that for a fixed wing in incompressible flow, L/D is strictly a function of geometry, not of weight or altitude. For the rotor, the L/D ratio is nearly constant, but maximum L/D increases slightly, from 21 to about 22. The small increase is caused by lift shifting to the efficient wing from the less efficient rotor. The difference between the wing only and rotor+wing narrows with airspeed for every altitude, but narrows less as altitude increases.

These results show that high altitude improves the performance of the wing and rotor independently but also shows that a transfer of lift from the rotor to the wing occurs. This transfer of lift to the efficient wing increases L/D performance and thus reduces power required.

Conclusions

The performance of slowed-rotor compound aircraft was calculated using the comprehensive analysis CAMRAD II. Correlation with historical high advance ratio test data demonstrated the applicability of CAMRAD II to rotors in such flight conditions. Detailed performance of a rotor similar to that

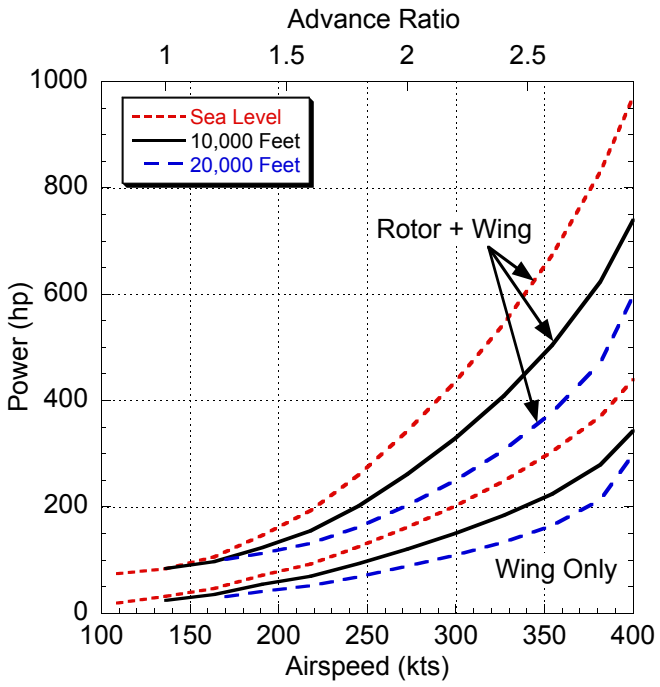

Fig. 33. Wing and total power from sea level to 20,000 feet, 0 deg collective, V_T = 230 ft/sec.

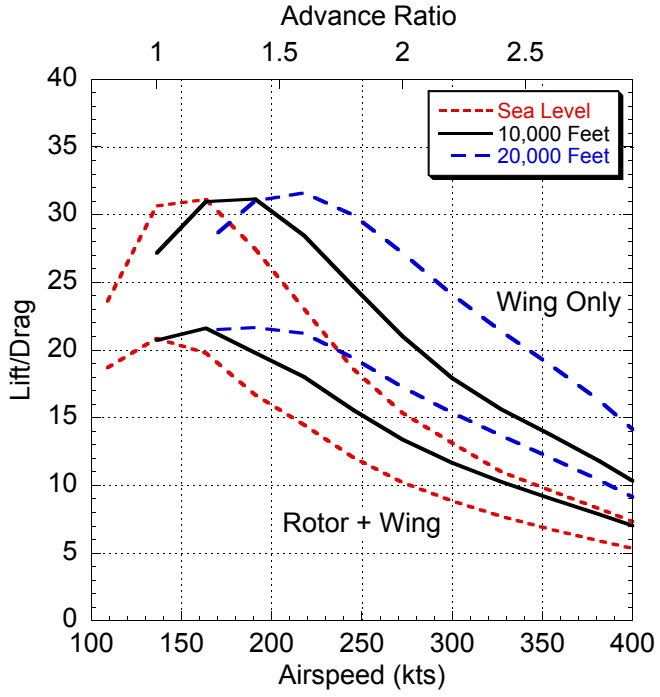

Fig. 34. L/D of rotor and wing from sea level to 20,000 feet, 0 deg collective, V_T = 230 ft/sec.

used on the CarterCopter Technology Demonstrator was presented. The rotor was analyzed as an isolated rotor and with a fixed wing. Specific conclusions follow.

1. CAMRAD II with a rigid wake model is able to capture performance trends of high speed rotors to at least an advance ratio of 1.45 although some offsets with the Jenkins data exist which could not be accounted for. Correlation was good with both the Jenkins and XV-1 isolated rotor test data.

2. For an autorotating rotor at high speed, slowing the rotor reduces the power required, whether the rotor is in isolation or in combination with a fixed wing.

3. The optimum collective for a high speed autorotating rotor is that which produces a small amount of positive thrust on the rotor. Negative thrust causes a reversal in the rotor flapping and trimmed shaft angles and substantially degrades performance.

4. For a combined rotor and wing at high advance ratio, there is a very narrow (1–2 deg) range of collective where an acceptable distribution of lift between the wing and rotor exists. Outside this range, the rotor and wing produce lift in opposite directions and increase the total vehicle drag.

5. Where there was beneficial sharing of lift between the rotor and wing, the wing carried most of the lift and hence rotor power was dominated by profile power. Induced power was generally small unless the wing and rotor produced opposite lift. Wing power was also dominated by profile power except at low speed where it was near stall.

6. The drag and power of the rotor for $M_{\text{TIP}} \leq 0.3$ were about the same as the wing. For $M_{\text{TIP}} = 0.4$, compressibility effects caused the rotor profile power to increase rapidly above 300 kts.

7. The separation between the wing and rotor for the model in this investigation was sufficient that there was negligible interference between the two at high speed.

8. High altitude resulted in a shift of lift from the rotor to the wing for zero collective and $M_{\text{TIP}} = 0.2$. The shift to the high efficiency wing, coupled with the reduced air density reduced the power required by more than 1/3 between sea level and 20,000 feet.

References

[1]Hohenemser, K., "A Type of Lifting Rotor with Inherent Stability," *Journal of the Aeronautical Sciences*, Vol. 17, September 1950.

[2]Hohenemser, K., "Remarks on the Unloaded Rotor Type of Convertiplane," Proceedings of the American Helicopter Society 11th Annual Forum, Washington, DC, April 1955.

[3]Hohenemser, K. H., “Some Aerodynamic and Dynamic Problems of the Compound Rotary-Fixed Wing Aircraft,” Proceedings of the American Helicopter Society 8th Annual Forum, Washington, DC, May 1952.

[4]Hohenemser, K. H., “Aerodynamic Aspects of the Unloaded Rotor Convertible Helicopter,” *Journal of the American Helicopter Society*, Vol. 2, (1), January 1957.

[5]Hickey, D. H., “Full-Scale Wind-Tunnel Tests of the Longitudinal Stability and Control Characteristics of the XV-1 Convertiplane in the Autorotating Flight Range,” NACA RM A55K21a, Ames Aeronautical Laboratory, May 1956.

[6]Marks, M. D., “Flight Test Development of the XV-1 Convertiplane,” *Journal of the American Helicopter Society*, Vol. 2, (1), January 1957.

[7]Johnson, W., “Rotorcraft Aeromechanics Applications of a Comprehensive Analysis,” Presented at Heli Japan 98: AHS International Meeting on Advanced Rotorcraft Technology and Disaster Relief, Japan, April 1998.

[8]Sweet, G. E., Jenkins Jr, J. L., and Winston, M. M., “Wind-Tunnel Measurements on a Lifting Rotor at High Thrust Coefficients and High Tip-Speed Ratios,” NASA TN D-2462, 1964.

[9]Jenkins Jr, J. L., “Wind-Tunnel Investigation of a Lifting Rotor Operating at Tip-Speed Ratios from 0.65 to 1.45,” NASA TN D-2628, February 1965.

[10]Hohenemser, K. H., “Full Scale Rotor Tests of the Air Force Convertiplane Model XV-1 in the NACA 40 x 80 Foot Wind Tunnel at Moffett Field, California,” McDonnell Aircraft Report 3379, McDonnell Aircraft Corporation, February 1954.

[11]Perisho, C. H. and de Garcia, H. J., “A Comparison of Detailed and Simplified Methods of Analysis of Rotor Stability in Forward Flight with Model Test Results,” Proceedings of the American Helicopter Society 18th Annual National Forum, Washington, DC, 1962.

[12]Abbott, I. H. and von Doenhoff, A. E., *Theory of Wing Sections*, Dover Publications, Inc., 1959.

[13]Carter Jr., J., “CarterCopter—A High Technology Gyroplane,” Proceedings of the American Society Vertical Lift Aircraft Design Conference, San Francisco, California, January 2000.